Artificial Neurons with Logical Properties Based on Paired-Band Microelectrode Assemblies

Christian Amatore,* Laurent Thouin, and Jean-Stéphane Warkocz[a]

Dedicated to Professor Allen J. Bard on the occasion of his 65th birthday

Abstract: Electrochemically operated devices based on paired-band microelectrode assemblies, which mimic the five basic physicochemical steps of neuronal processing of information (namely, propagation of electrical impulse along the emitting neuron to its synaptic cleft, release of chemical messenger in the synaptic cleft, diffusion of chemical messenger across the synaptic gap, detection of chemical messenger by the receiving neuron, propagation of electrical impulse along the receiving neuron), can be built by taking advantage of the unique properties of double-band electrodes. It is shown that such artificial neurons can be designed to perform as Boolean logical gates with AND or OR functionalities. The time responses of the devices and the basic theoretical features, which explain their unique properties, have been investigated analytically and through accurate conformal mapping simulations of the diffusional cross-talk operating in the vicinity of each coupled double-band assembly. These simulations are in complete agreement with experimental observations. Furthermore they allow a simple analogy to be established between the device at hand and a simple double band. Based on this analogy, simple analytical formulations of the response time of the system and of the limiting currents that can pass through the assembly are proposed. The relevance of the present results to other situations in which analogous physico–chemical phenomena operate is also discussed.

Keywords: electrochemistry · logic gates · oxidations · paired-band electrodes · reductions

Introduction

In nature, transmission of specific information often proceeds through a sequential combination of biochemical and physicochemical steps. A typical illustration of this delicate interplay between biochemical and physicochemical processes is given by the processing of information through a chain of interconnected neurons. Thus, the emitting neuron sends a potential impulse along its axon from its main cell body to its terminal synaptic clefts, through which the neuron is connected to the receiving neuron(s). This information proceeds along the axon through the sequential opening/closing of a series of ion channels. When this electrical stimulation reaches the synaptic area, it forces the release of chemical neurotransmitters into the synaptic cleft through a still debated sequence of biochemical events.[1] The released molecules (e.g., dopamine) diffuse through the synaptic cleft from the emitting neuron membrane surface to that of the receiving neuron, where they eventually activate a receptor site. This activation results in the creation of a second electrical impulse that now propagates along the membrane of the receiving neuron toward its main body, where it is processed and may be sent to other connected neurons of this chain.

Cast into physicochemical terms this whole process can be summarized by the following sequence of events: electrical perturbation (potential impulse); transduction into chemical perturbation (exocytosis of neurotransmitter); transmission of information by diffusion (diffusion into the synaptic cleft); transduction into a new electrical perturbation (detection and ensuing potential impulse).

It occurred to us that the same sequence of events could be repeated electrochemically at the micrometric scale taking advantage of the peculiar properties of paired-band microelectrodes.[2, 3] Thus electrical information can be shuttled through a chain formed by two artificial synapses connected by an artificial neuron, by repetition of the following electrochemical events: electrical potential stimulation →electrogeneration →diffusion →collection →new electrical stimulation. This can be readily adapted to perform with the functionality of a Boolean AND gate. Also, by use of another design, the initial electrical information can be sent into different geometrical directions according to its sign while it is processed through the assembly, so that the whole device performs with the properties of an OR Boolean logical gate. Here we report a series of experimental and theoretical evidence that establish the validity of these principles.[4]

[a] Dr. C. Amatore, Dr. L. Thouin, J.-S. Warkocz
Ecole Normale Supérieure, Département de Chimie
URA CNRS 1679, 24 rue Lhomond, F-75231 Paris Cedex 05 (France)
Fax: (+33) 1-4432-3863
E-mail: amatore@ens.fr

0947-6539/99/0502-0456 $ 17.50+.50/0

Results and Discussion

Principle of mimicked neuronal behavior: The device is outlined in Figure 1. Two double-band electrode assemblies[3b,e,g] (hereafter also called the two *synapses* by analogy with a biological neuron) are dipped in the same electrolyte

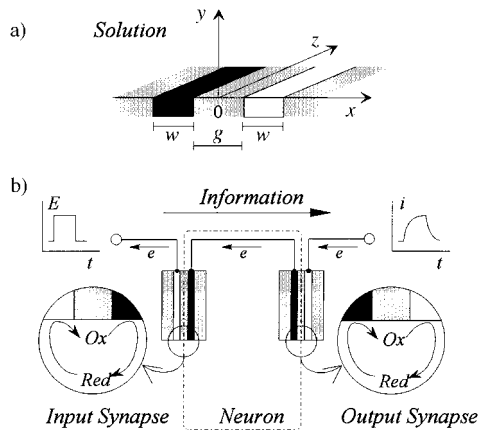

Figure 1. Schematic representation of the two double band assembly used in this work. a) Schematic view of a cross section of one of the double-band electrodes. b) Connections between the double bands and indication of the diffusional cross-talks existing near each double band (see text). The color code used for the electrodes (i.e., black or white) indicates only which electrodes are short-circuited and isolated from any power supply (black ones) and which ones are connected to the bipotentiostat (white ones) without implication on their nature (viz., anode or cathode).

solution containing, in our case, a molecular species (*Red*) under its stable reduced form, belonging to the chemically reversible redox couple *Red*/*Ox*. Two electrodes, one of each double band, are connected in short circuit through a conducting metallic lead isolated from the solution. The second electrode of one double band (input of the first synapse) may be submitted to a positive electrical potential square pulse, which activates the device by oxidation of species *Red*. The second band of the other double band (output of the second synapse) is biased at a potential set on the plateau of the reduction wave of the *Red*/*Ox* couple, in order to collect the information.

Before the incoming potential pulse is applied to the input of the first synapse, the ensemble of the two bands in short circuit is in electrochemical equilibrium with the solution containing species *Red* alone, and so both bands take the same potential as the solution. When the input of the first synapse is subjected to the oxidizing potential pulse, *Red* is oxidized at its surface and diffuses cylindrically into the solution.[3e–g] This way, a wave of oxidizing solution spreads toward the second band of the first synapse. When this diffusional wave reaches it, the solution surrounding the second band has a more positive potential than the metal so that the electrode tends to reduce it. To do so electrons must be shuttled from the band to the solution, which normally should be impossible, because the two short-circuited bands cannot acquire a positive charge without reaching an infinite positive potential, since they consist of a metallic conductor isolated from any electrical source. However, with the present system, the band in contact with the oxidizing solution in the first synapse may reduce it, provided an equivalent charge is compensated by the second synapse. This implies that the short-circuited band of the second synapse simultaneously oxidizes at the same rate the solution surrounding it. In other words, through microscopic loss of charge (vide infra, in the theoretical section), the ensemble of the two short-circuited bands adjusts its potential at a value intermediate between that of the oxidizing solution (created around the first synapse) and that of the still unaffected solution (around the second synapse). Under these conditions, the ensemble is reducing on one side (first synapse) and oxidizing on the other side (second synapse), and is therefore traversed by a current that corresponds to the identical amplitudes of the fluxes of charges exchanged at each short-circuited electrode. This way, macroscopic charges never develop in the isolated conductor and the system transfers the information imposed on its input band to the second synapse. This has two consequences which are exploited in this work (see also Morita et al.[5] for another interesting application of this principle in the field of trace analysis).

On the one hand, *Ox* is formed at the second synapse short-circuited electrode. As explained above for the first synapse, this creates a diffusional wave of oxidizing solution that moves toward the paired-band electrode of the same synapse. Since this electrode is poised on the reduction plateau of the *Red*/*Ox* couple, every *Ox* molecule reaching its surface is necessarily reduced into *Red* and a current necessarily flows through the overall device, which is another way to say that the initial information, namely, the potential square pulse applied to the input of the first synapse, has been processed by the *neuron* and transferred to the output of the second synapse. This transmission occurs necessarily with a time delay, since it is carried by diffusion.[3e–g] In fact (vide infra, theoretical section), this requires a duration in the order of $\tau = 4w^2/\{D[(1+w/g)^{1/2}-1]^2\}$, where D is the average diffusion coefficient of *Red* and *Ox* species, g the gap thicknesses, and w the common width of the band electrodes (see Figure 1a) used in each synapse.

On the other hand, it is important to recognize that each synapse behaves as a generator/collector paired-band assembly: *Red* is oxidized at the input band electrode of each synapse; the electrogenerated *Ox* species diffuses toward the corresponding output band of each synapse where it is reduced back to *Red*; the regenerated *Red* species diffuses back to the input band electrode where it restores the originally depleted *Red* concentration, and so on. In former works,[3e–g] we showed that this whole sequence rapidly creates (namely, only after a few τ) a steady state diffusion pattern in the vicinity of each paired-band assembly, with the consequence that ultimately identical currents flow at each paired band, and a negligible current escapes from the vicinity of the electrodes toward the counter electrode located far away into the bulk solution. It is thus understood that the whole device shuttles information from a squared pulse input through itself and performs this operation with a filtering behavior that is phenomenologically reminiscent of that of a first-order filter of the time constant τ.

To conclude this section, we wish to stress that to propagate a positive potential pulse, the two paired-band assemblies must be bathed by a solution containing the reduced form (*Red*) of a chemically reversible redox couple. Obviously, the converse is true for propagation of a negative potential pulse. This requirement can be used to address information in different directions based on the positive or negative nature of the potential pulse applied at the first synapse input. This OR function will be illustrated experimentally below. Similarly, this can be used to perform an AND function.

Experimental illustration

Mimicking neuronal synaptic behavior: Figure 2 shows the experimental response of a device such as the one described in the above section when the two artificial synapses were dipped into the same solution [here, 5 mM ferrocene (Fc) in MeCN/0.3 M NBu_4BF_4] and were submitted to a potential square pulse (here, 0.2 V to 0.8 V vs. SCE, see Figure 2a; $E^0_{Fc^+/Fc} = 0.43$ V vs. SCE) applied to the input band of the first assembly. Each synapse was composed of two paired platinum

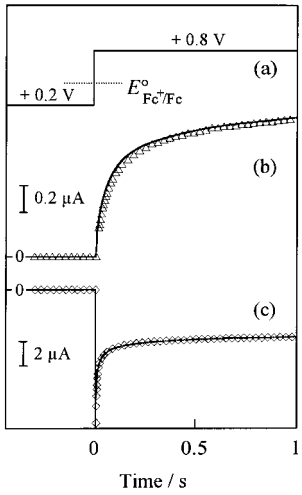

Figure 2. Processing of a positive potential step by the assembly schematized in Figure 1. Each double band-synapse consists of two platinum bands ($w = 6$ μm, $l \simeq 4$ mm) separated by an insulating gap in mylar ($g = 2$ μm) and dipped in a solution of ferrocene (5 mM in MeCN/0.3 M NBu_4BF_4). a) Potential pulse applied to the input of the first synapse. b) Current monitored at the output of the second synapse. c) Current monitored at the input of the first synapse. In b) and c) the experimental currents (symbols) are compared with the simulated ones (solid lines).

bands (thickness: $w = 6$ μm; length: $l \simeq 4$ mm) separated by an insulating gap ($g = 2$ μm) in mylar. Each assembly was from a cross section of an arrangement consisting of a mylar film sandwiched in between two platinum foils glued with epoxy resin (see Experimental Section for determination of the dimensions of electrodes and gap). The two assemblies were set up a few centimeters apart in the solution, one electrode of each being connected in short-circuit by an insulated copper wire of approximately 15 cm overall length.

Figure 2b represents the current flow through the output band of the second synapse, shown in phase with the potential pulse (see Figure 2a) applied to first synapse input. As explained above, the output current rise is filtered with a time constant of about 100 ms, a value which compares satisfactorily with the predicted time constant (vide infra); $\tau = (g^2/D)\{4(w/g)^2/[(1 + w/g)^{1/2} - 1]^2\} \simeq 80$ ms for $D_{Fc} = 1.8 \times 10^{-5}$ cm^2 s^{-1}, $w = 6$ μm and $g = 2$ μm.

At the beginning of the current rise period, the diffusion layers are too small to allow a total cross-talk between the two paired electrodes of each synapse. This is best observed upon examination of the current flowing through the lead connected to the input electrode of the first synapse (Figure 2c). Initially, most of the *Ox* (Ferricinium, Fc^+) flux electrogenerated at the input electrode of the first synapse is not collected by its paired electrode, so that the current flowing through this lead has an important Cottrellian nature; most of the current flow escapes into the solution bulk toward the counter electrode. However, the noncollected fraction of the flux decreases when time becomes longer than τ, because then the diffusion layers sizes are sufficient to allow a significant cross-talk between the paired electrodes within each synapse and therefore between the two synapses (vide supra). Thus, the Cottrellianlike fraction of the current vanishes progressively, being replaced by a steady state current that features the setting-up of an extensive diffusional cross-talk between the paired-band electrodes within each synapse. Thus as time reaches infinity (vide infra), the current in the input lead is expected to tend toward a constant value, which is the same as the one flowing through the output lead of the second synapse. Under these conditions the whole information about the current is shuttled through the assembly.

When the potential pulse ends, the input band electrode becomes reducing versus Fc^+, so that all the Fc^+ carriers are consumed at each electrode of the device and the current drops to zero, thus terminating the processing of the information. This occurs again with a diffusional time constant τ (data not shown; compare with Figure 4).

Mimicking neuronal synaptic behavior with OR or AND Boolean properties: The above device has phenomenological properties that could be achieved using a single double-band.[3e–g] Indeed, each synapse behaves almost identically, albeit for different physicochemical reasons. Therefore, the use of two synapses seems to complicate unnecessarily the system and even to increase its time constant as compared with a single synapse (vide infra). However, the use of a device with two synapses allows us to modulate the properties of the whole system, so that it can execute Boolean functions while it processes the information. The nature of the Boolean function is determined by the solutions surrounding each synapse and by the connections within the system. We wish to illustrate this original property by showing how AND and OR functions can be performed.

AND logic gate: We have explained above that in order to perform, the two synapses must be bathed by solutions of identical redox status, for example, two solutions containing the reduced form of a chemically reversible redox couple. This situation (noted hereafter *Red-Red*) was shown to transfer positive pulses. Respectively, two solutions containing the oxidized form of a chemically reversible redox couple (noted *Ox-Ox*) allow the transfer of a negative pulse. If now two solutions of different redox nature are used in each synapse

0947-6539/99/0502-0458 $ 17.50+.50/0 *Chem. Eur. J.* **1999**, *5*, No. 2

vicinity, namely, *Red-Ox* or *Ox-Red*, the information cannot be processed because the short-circuited electrodes can only be cathode–cathode (*Red-Ox*) or anode–anode (*Ox-Red*). Passage of any significant current requires the build-up of macroscopic charges in the short-circuited electrode assembly, and this is impossible in an isolated metallic conductor. Because of this property the above device may perform an AND Boolean function; current passes when the two solutions are of identical redox nature (vide supra) and is blocked when the redox nature of the two solution differs. This property will be experimentally checked in the following, since it can also be used for the creation of a OR gate (vide infra).

OR logic gate: This function requires three synapses; one input and two output (see Figure 3). The input synapse is dipped in a solution containing two species, Red_1 and Ox_2, belonging to two different chemically reversible redox

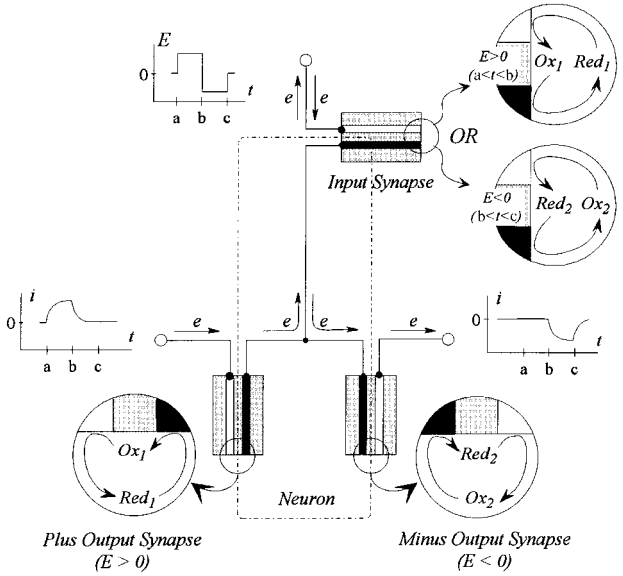

Figure 3. Schematic representation of a Boolean OR gate after the same fashion used in Figure 1; the three electrodes represented in white (one per synapse) are driven by a tripotentiostat, and the three electrodes represented in black (one per synapse) are short-circuited and isolated from any power supply. Each double band is dipped in a different solution contained in an independent vessel; the three solutions are connected by electrolyte bridges to ensure closing of the circuits loops. Input synapse, top; plus output synapse, bottom left; minus output synapse, bottom right.

couples, Red_1/Ox_1 and Red_2/Ox_2. Again, one electrode of this synapse is connected to a potentiostat and may be subjected to potential pulses, while the second electrode is short-circuited with two others electrodes, one per each of the two output synapses. One output synapse (plus output) is designed to process the positive signal information. It is therefore dipped into a solution containing only Red_1; its second electrode is poised on the plateau of the reduction wave of Ox_1. The other synapse (minus output), which is aimed to process the negative information, is soaked into a solution of Ox_2 only; its second electrode is biased at a potential set on the oxidation plateau of Red_2.

With this arrangement, when a positive potential is applied to the input electrode of the input synapse, it is processed through the plus output according to the same physicochemical processes described above, while a negative potential signal is obviously shuttled through the minus output. A positive pulse cannot be processed through the minus output, because this requires the presence of a species to oxidize in the second synapse. The converse is true for the plus output, which lacking the presence of a species to reduce in the second synapse cannot process a negative potential pulse. Therefore the above system processes the potential signal applied to its input with the properties of a OR gate; it directs the information towards one of its two outputs according to the sign of the potential perturbation. The physicochemical phenomena that sustain the processing of information are identical to those described above, therefore the transmission is again filtered with a time constant τ (vide supra). Figure 4 establishes the experimental validity of this system with

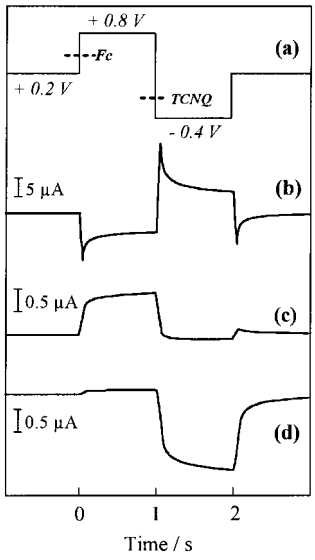

Figure 4. Processing of a potential signal by the Boolean OR gate schematized in Figure 3. All three double bands are as described in Figure 2. The input synapse was dipped in a solution containing ferrocene (5 mM) and TCNQ (5 mM) in MeCN/0.3 M NBu_4BF_4. The plus output synapse was dipped in a solution of ferrocene (5 mM) in MeCN/0.3 M NBu_4BF_4, and the minus output synapse in a solution of TCNQ (5 mM) in MeCN/0.3 M NBu_4BF_4. a) Potential signal applied to the input band of the input synapse. b) Current monitored at the input of the input synapse. c) Current monitored at the plus output. d) Current monitored at the minus output.

ferrocene (Red_1) and TCNQ (Ox_2; $E^0_{TCNQ^-/TCNQ} = -0.08$ V vs. SCE). It is seen that when the system is submitted to a double potential step (+0.2 to +0.8 to −0.4 V vs. SCE, Figure 4a), a current always passes through the input synapse, because ferrocene is oxidized during the positive step, while TCNQ is reduced during the negative one. The input current is then positive during the positive potential step and negative during the negative step (Figure 4b; compare Figure 2c). However, only the positive current may be transferred at the plus output, which contains ferrocene (Figure 4c), and only the negative one may reach the minus output, that is, that containing TCNQ (Figure 4d). Inspection of the rising or descending sections in Figures 4c and 4d shows that the response time is as expected comparable to those in Figure 2c (ca. $\tau = 0.1$ s), and therefore are in qualitative agreement with the predictions.

Theory: Figures 2 and 4 establish qualitatively the experimental validity of the principles that have been developed above. Information can be processed and possibly treated logically by these double-band assemblies in a way that mimics biological neurons operation. One key feature in the processing of any information is the time response of the transferring device. As observed experimentally, the time response is governed by the occurence of a significant diffusional cross-talk between the two bands paired within each synapse. A quantitative evaluation of the time constant of the assembly can be achieved by simulation of the diffusional cross-talk in the series of two synapses considered above. These simulations were performed in the conformal space of the device to take advantage of the great simplification of the problem at hand as established previously for double- and triple-band electrodes.[2, 3e,f]

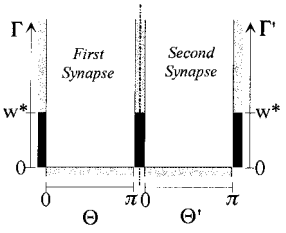

Figure 5. Conformal space transform of the assembly in Figure 1 (see text and appendix for equation of the transformation). The two conformal spaces (i.e., (Γ,θ) for the first synapse and (Γ',θ') for the second synapse) are represented side to side; the two short-circuited electrodes in Figure 1 are represented by a single boundary with two sides. Transformed electrodes are represented in solid black and transformed insulators in dotted areas.

In the conformal space[2, 3c,e,f] (see Appendix and Figure 5), the natural geometrical arrangement of a double synapse is transformed into a system consisting of two adjacent rectangular boxes. This transformed geometry smooths all the important curvatures of the concentration profiles that exist in the true space near the electrode edges and over the gap region of each synapse (vide infra and Figure 7). This allows a facile and rapid numerical resolution of Fick's laws in the conformal space by techniques that have been previously elaborated and well documented for double- and triple-band electrode assemblies.[2, 3e,f]

Through this procedure, the current response of the double-synapse assembly discussed above can be determined and compared with the experimental ones. This is performed in Figure 2 for the output current (namely, that flowing through the output lead of the output synapse; Figure 2b) and the input current (namely, that flowing through the input lead of the input synapse; Figure 2c) for ferrocene ($D_{Fc}=1.8\times 10^{-5}\,cm^2\,s^{-1}$, $E^0_{Fc^+/Fc}=0.43$ V vs. SCE) used in an assembly of two synapses (Figure 1b) with $g=2$ μm, $w=6$ μm, and $l=3.9$ mm (first synapse) or $l=4.2$ mm (second synapse) submitted to a potential square pulse. As evidenced by Figures 2b and 2c the agreement is excellent (current magnitudes and time constant), which quantitatively validates all the above discussions.

Simulations allow a more careful investigation of the behavior of the system over a longer time. Indeed, it is apparent from Figures 2 and 4 that the output current rises rather sharply with a time constant in the order of τ. Afterwards it still increases steadily with time, but at a considerably slower pace. This is evidenced in Figure 6a, which represents the experimental output current with a logarithmic time scale when the input potential signal is a step function (from 0.2 to +0.8 V vs. SCE at time zero and maintained at 0.8 V for more than 100 s). This figure shows that after a fast initial rise, the output current increases almost linearly with log(t) up to a steady state value that is reached after about 20 s. Such a behavior is expectable considering the diffusional properties of paired-band assemblies, albeit we have not discussed it up to now.

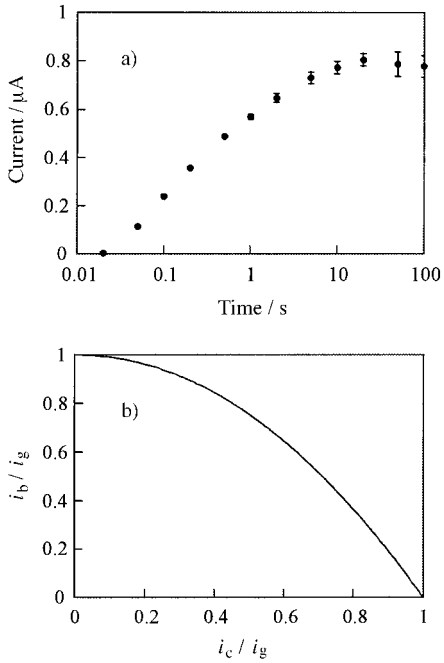

Figure 6. Behavior of the system in Figures 1 and 2 over a longer time. a) experimental variations of the output current with time for conditions identical as in Figure 2 except for the duration of the potential step pulse (100 s here; see text). b) Simulated variations of the amplification factor i_g/i_b and collection factor i_c/i_g [see text and Eq. (2)] when neglecting the interference of convection.

Indeed, with a double-band electrode used in the generator–collector mode (as each of the two synapses in series) pure steady state is achieved theoretically only at after an infinite time, because steady-state achievement requires that the diffusional leak of the species electrogenerated at the generator electrode toward the solution bulk becomes negligible versus the generator current. In fact we established previously for double-band assemblies[2, 3e] that whenever the time scale exceeds $(g+w)^2/D$ significantly the generator current i_g and the collector current i_c are related through the relationship given in Equation (1), in which i_b is the current at a single-band electrode of identical dimensions as each of the paired bands (i.e., the generator current when the collector electrode is not connected).

$$i_b/i_g = 1-(i_c/i_g)^{2.01} \quad (1)$$

Since i_b, the single-band current, decays logarithmically with time, steady state is approached in a logarithmic fashion and is reached only at infinity; theoretically one has then $i_b^\infty = 0$ and therefore $i_c^\infty = i_g^\infty$ [Eq. (1)]. However, this theoretical feature cannot be observed experimentally, because it supposes a diffusional transport only, while at longer times

0947-6539/99/0502-0460 $ 17.50+.50/0 *Chem. Eur. J.* **1999**, *5*, No. 2

convection interference cannot be ignored.[6] The effect of convection becomes experimentally apparent when the diffusion layer thickness (which increases with time like $\log(t)$ for band electrodes) becomes comparable with that of the *convection free* hydrodynamic layer.[7] For our experimental conditions this occurs after a few seconds. At times longer than a few seconds, the leakage of the species electrogenerated at the generator electrode toward the solution bulk does not occur only by diffusion, but also becomes controlled by convection. As a consequence i_b i) tends to become independent of time above a few seconds and ii) has a larger value than it would have if controlled by diffusion only. As a result, at infinite times a convective steady state is achieved, in which i_b [Eq. (1)] becomes constant, but is not zero so that the collector and generator currents also become constant yet with $i_c^\infty < i_g^\infty$ [Eq. (1)].

The same phenomenology obviously applies to the series of two synapses considered here; however owing to the slight complication of diffusion cross-talk due to the presence of two synapses, Equation (1) needs to be replaced by Equation (2) [Figure 6b] as established by simulation in the conformal map space.

$$i_b/i_g = 1 - (i_c/i_g)^{2.03} \qquad (2)$$

This equation is very close to Equation (1) and differs only by the slight modification in the exponent of i_c/i_g. This close similarity can be understood easily by considering the diffusional situation in the conformal space[2] (Figures 5 and 7).

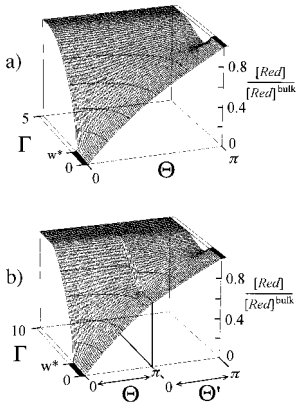

Figure 7. Comparison between the concentration profiles in the conformal spaces for a) a double band operated in the generator–collector mode, and b) a two-synapse assembly (Figure 1) with the same double bands, when the two systems approach steady state [Eq. (1) and Eq. (2), respectively]. The concentration profiles are shown in both cases at $t = 85\tau$, with $\tau = g^2/D$ in a) and $\tau = (g^{eq})^2/D$ in b) [g^{eq} is given in Eq. (5)].

On the one hand, Figure 7b shows that the boundary featuring the two short-circuited electrodes in the middle of the diagram (Figure 5) functions nearly as a hole allowing communication between the two sub-boxes featuring each synaptic compartment. Indeed, since the two short-circuited electrodes are necessarily at the same potential, identical concentrations are maintained on each side of the boundary. Also, since these electrodes cannot accumulate charges, the moduli of the integrated current fluxes must be the same on each side of the boundary, so that the average concentration gradients over the boundary are identical on each side. (Note that this is no more true for the $\Gamma > w^*$ section of the boundary, which represents the insulating sections. Then concentrations on each side may differ; however, the concentration gradients are necessarily equal at each Γ value, since they are zero.

On the other hand, it is known that most of the behavior of double-band assemblies is governed by diffusion in the near vicinity of the electrodes[2, 3e,f], that is, at $\Gamma \geq w^*$ in the conformal space. Considering the above, this shows that the diffusion pattern in the conformal space featuring the two-synapses assembly closely resembles that which would be obtained for a single double-band element performing in a generator–collector mode,[2, 3e] in which the generator is the input band electrode of the input synapse and the collector the output band of the output synapse. This close identity is adequately seen by inspection of Figure 7 which compares the concentration profiles of the *Red* species for a double band (Figure 7a) with the assembly of the two synapses (Figure 7b) in their conformal spaces. However, the match is not exact i) because of the presence of the insulating boundary in the middle of the diagram for $\Gamma > w^*$ and ii) because although the integrals of the current densities (i.e., the concentration gradients) over the $[0,w^*]$ interval of Γ are identical, the current densities themselves are not equal for a given value of Γ. This explains why Equation (2) is extremely close to Equation (1), but cannot be strictly identical.

The above analogy presents other interesting points. First, because of this near equivalence, when the steady state is approached the concentrations of *Red* and *Ox* in the middle boundary plane are necessarily equal, that is, $[Red] = [Ox] = [Red]^{bulk}/2$, where $[Red]^{bulk}$ is the initial bulk concentration of *Red* in each synaptic compartment. Indeed, the concentration gradients versus θ of *Red* and *Ox* in a double-band system operating near to the steady state in generator–collector mode are constant in the conformal space, in the region located between the two transformed electrodes. With the concentration of *Red* being zero at the input electrode and that of *Ox* being zero at the output electrode, and since $[Red] + [Ox] = [Red]^{bulk}$ at each point of the solution, the above equality ensues easily. Because of the Nernst law, this establishes that when steady state is approached, the short-circuited electrodes are poised at a potential equal to the standard potential E^0 of the redox couple.

Second, because at steady state $[Red] = [Ox] = [Red]^{bulk}/2$ in the middle boundary plane of the conformal space, we can readily deduced that the steady-state current limit of the assembly is approximately equal to half that observed when one of the synapses is operated alone in a generator–collector model[2, 3e] [Equation (3), in which the subscript db stands for

$$i_g^{stst} = i_c^{stst} \approx (i_g^{stst})_{db}/2 = (i_c^{stst})_{db}/2 = nFD[Red]^{bulk}\, 1 \times \frac{(\sqrt{-1}) \int_{g/2}^{w+g/2} [(\eta^2 - g^2/4)(\eta^2 - \{w + g/2\}^2]^{-1/2}\, d\eta}{2 \int_{-g/2}^{g/2} [(\eta^2 - g^2/4)(\eta^2 - \{w + g/2\}^2]^{-1/2}\, d\eta} \qquad (3)$$

a single double-band synapse and the superscript stst indicates the steady-state limit].

The third consequence of this near equivalence deals with the analytical evaluation of the time response of the assembly. The equivalent double band has a transformed gap width that is double of that of each transformed synapse. Since homothetic scaling is allowed in the transformed space,[2] this is akin to say that the equivalent double band has the same gap width as each band in the transformed space, but that the widths of its transformed electrodes are half those of each transformed synapses. Because of the conformal transformations (see Appendix) this equivalence is expressed by Equation (4) in which g^{eq} is the gap width in the real space of the double band equivalent to the two-synapse assembly.

$$\mathrm{Argcosh}(1+2w/g^{eq}) = (1/2)\mathrm{Argcosh}(1+2w/g) \quad (4)$$

$$g^{eq} = g \times \{2(w/g)/[(1+w/g)^{1/2}-1]\} \quad (5)$$

$$\tau = (g^{eq})^2/D = (g^2/D) \times \{4(w/g)^2/[(1+w/g)^{1/2}-1]^2\} \quad (6)$$

Equation (4) readily affords g^{eq} [Eq. (5)]. Also, the response time τ of the two-synapse assembly is readily given by the duration of diffusion over the gap of the equivalent double band[2, 3e] [Eq. (6)], that is, precisely what has been observed experimentally (vide supra). Note that since $\tau_b = g^2/D$ is the time constant due to each individual synapses, $\gamma = 4(w/g)^2/[(1+w/g)^{1/2}-1]^2$, the bracketed expression in Equation (6) represents the delaying effect (note that one has always $\gamma > 16$) due to the setting-up of significant cross-talk between each synapse as compared with the transmission time (i.e., g^2/D[2, 3e]) when each synapse is operated alone. It is noteworthy that γ depends on w/g only, so that the delaying effect can be adjusted at will from its minimum value ($\gamma \sim 16$ and $\tau \sim 16g^2/D$, for $w/g \ll 1$) to larger values ($\gamma \sim 4w/g$ and $\tau \sim 4wg/D$, for $w/g \gg 1$) by modifying w/g while τ_b depends only on the gap and diffusivity of the electroactive material.

Relevant applications: In this last section we wish to discuss some relevant applications of the concepts and devices developed here (see also refs. [5a,b] for another interesting application in the field of trace analysis).

An immediate application of the concepts developed here is that they afford a simple interpretation of peculiar phenomena observed in scanning electrochemical microscopy (SECM).[8] In SECM, an ultramicroelectrode is dipped into a solution containing an electrochemically active species (e.g., *Red* in the above) at concentration C^0 and is used as a tip moved above the surface to be explored. When the electrode diffusion layer is not occulted by the object, and the electrode potential poised on the plateau of the oxidation wave of *Red*, the steady state current is given by Equation (7)[2] for a disc electrode of radius r_0.

$$i_{disc}^{stst} = 4nFr_0DC^0 \quad (7)$$

However, when the diffusion layer is partially occulted by the object (Figure 8a), diffusion of *Red* is hampered and the current is then smaller than predicted in Equation (7). Through this procedure, topology of objects can be mapped with a resolution that approaches the size of the electrode tip.[8b,c] However, what precedes is true only when the scanned object is insulating and therefore cannot act as an electrode. When the object scanned is sufficiently conducting so as to perform as a potential electrode, one observes a current amplification instead of a current decay whenever the object protrudes in the diffusion layer of the electrode.[8b,c] This peculiarity has been thoroughly explained by simulations in Bard's group,[8b,c] however the present work offers a simple explanation of the phenomena operating under these circumstances. Indeed, provided the intruding object is a conductor, the electrode tip and the part of the object encroaching upon the diffusion layer constitutes a synapse akin to those considered here. Thus, the part of conducting object contained in the synapse operates as a cathode (i.e., reduces *Ox*) which forces it, on the edges of the synapse, to behave as an anode and oxidize *Red* (Figure 8b). Since steady state current at a disc electrode originates mainly from the electrode perimeter, the situation is then equivalent to the creation of a fake disc electrode, larger than the size of the SECM probe, located on the object scanned, which oxidizes *Red*. Because this fake electrode has a radius R_0 necessarily larger than r_0, that of the true electrode tip, it can be seen from Equation (7) that the current is necessarily larger than when the conducting object does not encroach upon the tip diffusion layer as observed experimentally.

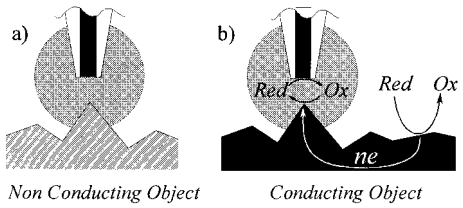

Figure 8. Schematic representation of scanning electrochemical microscopy (SECM) in relevance with the two-synapse assemblies considered in this work. The circle around the SECM tip electrode represents the size of its diffusion layer, that is, the maximum region of space that is probed by the electrode. a) Principle of current tip decrease when a nonconducting object protrudes into the diffusion layer and hampers diffusion to the tip. b) Principle of current tip enhancement when a conducting object protrudes into the diffusion layer (see text).

A second application which can be foreseen is related to sensing devices. Indeed, the response time and steady state currents of the two-synapse assemblies considered here depend on the medium bathing the synapses through the involvement of D (vide infra) in the expression for τ [Eq. (6)]. Here to minimize the experimental difficulties and also to simplify the system we used classical solutions possibly connected by bridges when they were different (see AND and OR Boolean gates and Experimental Section). An interesting alternative would consist of the use of polymers or polyelectrolytes around each synapse. Thus the transmission properties of the two-synapse assemblies would change according to the physicochemical status of the polymeric solutions around each electrode, because this status would control the diffusivity and the amount of electroactive species in the vicinity of the synapse. Based on this, a synaptic

0947-6539/99/0502-0462 $ 17.50+.50/0 *Chem. Eur. J.* **1999**, *5*, No. 2

nose could be designed to sense chemical species in a way similar to recently developed artificial noses,[9] but with the advantage of offering much more degrees of variations and in particular the possibility of an internal logical treatment by the device itself. Work is under progress in this direction in our group.

A third application which can be foreseen involves the learning aptitudes of the devices. To simplify the problem at hand, we have used solutions containing an excess of supporting electrolyte. Indeed, under such circumstances, transport of molecules occur by diffusion only because migration is suppressed.[7] If polymer is used around each synapse and as well as low excesses of supporting electrolyte, migration must control the transmission properties of the assemblies. Thus, starting from a situation in which no excess of electrolyte is present in the polymer surrounding the synapses, the assembly should not be able to transmit any significant information during a first stimulation. However, passage of this feeble information should nevertheless enrich the synaptic range in electrolyte[6, 10] so that transmission of a second pulse should be facilitated, and so on. In other words, the device is expected to learn to pass the information through the passage of the information itself in a way that is reminiscent of learning abilities of real neurons. Work is also under progress in this direction in our group.

Conclusion

In this work we have demonstrated that devices designed on the basis of double-band assemblies can mimic the five basic steps of neuronal transmission: electrical stimulation of emitting neuron →release of chemical messengers →diffusion of chemical messengers →detection of chemical messengers →electrical stimulation of receiving neuron. Thus, a potential pulse may be processed through an assembly of two coupled double-band electrodes, each with one short-circuited electrode. Each double-band performs as a synapse, and the two short-circuited electrodes as the neuron body. These simple systems can be adapted to acquire the properties of AND or OR logical gates.

The time responses of the devices and the basic theoretical features supporting their properties have been investigated by undertaking a complete simulation of the diffusional cross-talk operating in the vicinity of each coupled double-band assembly. These simulations, based on conformal mapping, provide results that are in complete agreement with the experimental observations. Furthermore they allow us to establish a simple analogy between the system at hand and a simple double band. Based on this analogy, simple analytical formulations of the response time of the device and of the limiting currents that can pass through the assembly have been achieved. Finally some potential applications of these assemblies have been discussed, particularly in the context of artificial nose or learning devices; however, these are still in development in our laboratory.

Experimental Section

Chemicals: Solutions of ferrocene (Fc, Merck) and/or tetracyanoquinodimethane (TCNQ, Sigma) were prepared in acetonitrile (Carlo Erba, HPLC grade) containing 0.3 M tetrabutylammonium tetrafluoroborate (NBu_4BF_4). NBu_4BF_4 was synthesized by mixing aqueous solution of NBu_4HSO_4 and $NaBF_4$ (Aldrich). The precipitate was extracted with dichloromethane (Merck), recrystallized from ethyl acetate/petroleum ether and dried under vacuum. Before use, the solvent was heated over calcium hydride and then distilled under N_2 atmosphere.

Double-band electrodes: The double-band assemblies were prepared according to a previously reported procedure[3b, 11] by placing a mylar film (2.5 μm nominal thickness, Energy Beam Sciences) as an insulator between two sheets of platinum foil, with the whole inserted between two pieces of soft glass. The platinum foils were purchased from Goodfellow (5 μm nominal thickness). These materials were sealed by applying a small amount of epoxy resin (Epon 828 with 10% triethylentretramine, Aldrich) between all layers. Pressure was applied to the assembly with a clip to keep the spacing between the layers as small as possible and the epoxy sealing as tight as possible. The curing process was carried out at a temperature of 120 °C for 2 h. Electrical connections were made independently to the back of each foil with silver epoxy (Elecolit, type 340) before completing the double-band device by sealing the whole assembly into a glass tube. A cross section of this assembly was then exposed with a diamond saw and polished by successive steps with five abrasive papers of finer and finer grades (Presi P400, P600, P1000, P1200 and P4000). The final polishing step was performed on wet tissue (Presi NV) with alumina (Presi, 0.3 μm grain size) and surface controlled under an Olympus binocular equipped with a video camera. It was apparent from the photographs that albeit the parallelism of the bands was always excellent, in some assemblies used here the bands were misaligned lengthwise by a maximum of 3% (over a 4 mm typical length). Band widths and gap were evaluated from photographs taken with an Olympus microscope calibrated with 10 μm divisions. For each double-band assembly, these dimensions (e.g., gap, electrode widths, and electrode lengths—values reported in the text) were then determined more precisely by finely adjusting these parameters through the simulation of voltammograms obtained for each electrode and with different scan rates so as to obtain the best fits with a single set of parameters at all scan rates. In this adjustment procedure, the initial values were the nominal values (gap and band thicknesses) or those obtained by optical measurements (electrodes lengths). The diffusion coefficient of ferrocene (5 mM) in our medium has been estimated by the use of a Pt disk microelectrode (12.5 μm radius based on independent calibration) leading to a value of $D_{Fc} = 1.8 \times 10^{-5}\ cm^2 s^{-1}$.

Instrumentation: Experiments were conducted at room temperature under argon atmosphere after complete degassing of the solutions by argon bubbling. The cell (ca. 15 mL) was equipped with about a 1 cm^2 apparent surface area platinum counter electrode and a Tacussel SCE reference electrode. Potential control of one band electrode of each synapse (see text and Figures 1 and 3) was achieved by a locally constructed bipotentiostat (viz., four-electrode cell; two working electrodes, one reference electrode, one counter electrode in the system represented in Figure 1) or by a locally constructed tripotentiostat (viz., five-electrode cell; three working electrodes, one reference electrode, one counter electrode in the system represented in Figure 3) controlled by a EGG & PAR waveform generator (model 175). In all experiments except in those dealing with the OR application (Figure 3), the two double bands were dipped in the same solution and were placed a few centimeters apart to avoid any direct communication. For the OR application, the cell consisted of three independent cylindrical vessels interconnected by fine sintered glass bridges to allow electrical connection, but prevent solution mixing. Each vessel was filled with a different solution (see text and Figure 3) and contained a single double-band electrode. Connections between the three double-band electrodes are detailed in the text and in Figure 3. Voltammograms and chronoamperograms were recorded on a Nicolet 320 digital oscilloscope and transferred to a PC for data processing.

Simulations: Programs were written in Pascal and the simulations were performed on a Pentium PC. All simulations were performed in the conformal spaces of the system at hand through algorithms adapted from previously described ones,[3e–g] based on the analysis presented in the Appendix. The only difficulty was related to the consequences of the

misalignment of paired bands. For introducing this effect, each paired-band assembly was separated theoretically into three individual components and treated by summating the currents due to each of these three individual components. A first component is the section of the generator not flanked by the collector. This was treated at a single-band electrode. The second component was that in which the generator is flanked by the collector and which was therefore treated as a double band. The third component was that consisting of the fraction of the collector not flanked by the generator, for which the current was set to zero because no collection could exist. Mathematically this decomposition is correct except within the micrometric zones, which are the boundaries between the three sections. However, the errors associated to these neglected zones are at most equivalent to those associated to the neglecting of edge effects and therefore are fully negligible.[3e–g]

Appendix

Simulations in the conformal space: Derivation of conformal space and simulations of diffusion at double bands alone were performed as described previously.[2, 3e–g] Derivation of conformal space and simulations of the double-band assemblies follow readily from this previous work so that we report here only a brief summary and principle of the method. Straight notations (viz., x, y, for the true space, Figure 1a; Γ, θ, for the conformal space, Figure 5) are used for the space variables in the first synapse, while primed ones (viz., x', y', Γ', and θ') are used in the second synapse. For each synapse, the conformal transformations and equations are identical except for the boundary conditions at electrode surface, which depend on the synapse, so that these are described here for the first synapse only, while boundary conditions will be given for each individual synapse.

The following dimensionless variables are defined as follows: $a = [Red]/[Red]^{bulk}$ (concentration) and $\lambda = t/T$ (time), in which T is the maximum duration of the electrochemical experiment and the others parameters are defined in the text. Then the subsequent transformations were achieved on the natural space variables (x, y) to introduce the conformal space (Γ, θ):[2, 3e–g] $x = g/2\ \cosh(\Gamma)\sin(\theta)$ and $y = g/2\cosh(\theta)\sin(\Gamma)$. This allows us to recast Fick's second law [Eq. (8)], which is valid in the natural space,[7] (note that a single Fick's law is required since $[Ox] = [Red]^{bulk} - [Red]$, because of mass conservation) into Equation (9), which is valid in the conformal space[2, 3e–g] ($b = [Ox]/[Red]^{bulk} = 1 - a$).

$$\frac{\partial[Red]}{\partial t} = D\left(\frac{\partial^2[Red]}{\partial x^2} + \frac{\partial^2[Red]}{\partial y^2}\right) \tag{8}$$

$$\frac{\partial a}{\mathrm{d}\lambda} = D^*\left(\frac{\partial^2 a}{\partial \Gamma^2} + \frac{\partial^2 a}{\partial \theta^2}\right) \tag{9}$$

$$D^* = \frac{1}{p^2}\ \frac{1}{(\sinh^2\Gamma\ +\ \sin^2\theta)} \tag{10}$$

In Equation (10) $p = g/2(DT)^{1/2}$. Within the conformal space, the gap thickness is π (i.e., $\Gamma = 0,\ 0 \le \theta \le \pi$) while the electrode widths are $w^* = \mathrm{Argcosh}(1 + 2\gamma)$, in which $\gamma = w/g$, that is, the transformed electrodes correspond to $\theta = 0$ or π, $0 \le \Gamma' \le w^*$.

The above partial derivative equation was then made discreet and solved by numerical finite differences according to procedures we previously reported and by the Hopscotch method.[3e–g] These numerical procedures afford the values of a at any required mesh point of the two simulation grids used (one for each synapse) for any time $\lambda + \Delta\lambda$ based on those determined at time λ, where $\Delta\lambda$ is the time increment in the simulation, except for the mesh points located on the boundaries (viz., $\theta = 0$ or π, $\Gamma = 0$ or ∞, first synapse; $\theta' = 0$ or π, $\Gamma' = 0$ or ∞, second synapse). To determine the a values on the boundaries one must use the proper set of boundary conditions at each transformed electrode and at each transformed insulating wall, as well as at infinity ($a = 1$, for $\Gamma \to \infty$). Therefore, starting from the situation at time zero ($\lambda = 0$, $a = 1$ at each mesh point of each grid), a values can be determined iteratively at any point of space for any value of λ of the time and in particular at $\lambda = 1$ (viz., $t = T$).

At each insulating wall ($\theta = 0$ or π, $w^* < \Gamma$) a zero flux boundary condition applies: $\partial a/\partial\theta = 0$. The same is true over the gap ($\Gamma = 0,\ 0 \le \theta \le \pi$): $\partial a/\partial\Gamma = 0$. At infinity, the solution is not affected by diffusion so that $a \to 1$ when $\Gamma \to \infty$.

The boundary conditions at the electrode surface are more delicate, since they depend on the electrode considered. At the input electrode of the first synapse, the potential E is imposed externally. Considering a Nernst law with $a + b = 1$, one obtains for $\theta = 0,\ 0 < \Gamma < w^*$: $a = 1/[1 + \exp(\xi)]$, in which $\xi = (nF/RT)(E^0 - E)$ and n is the number of electrons transferred in the Red/Ox couple and E^0 its standard potential. At the output of the second synapse, the potential is set on the plateau of Ox reduction wave (viz., $b = 0$), so that for $\theta' = \pi,\ 0 \le \Gamma' \le w^*$: $a = 1$. The conditions on the short-circuited electrodes ($\theta = \pi,\ 0 \le \Gamma \le w^*$, first synapse and $\theta' = 0,\ 0 \le \Gamma' \le w^*$, second synapse) are implicit, because on the one hand a is constant all over the two electrodes, since these are at an equipotential surface, that is, for $\theta = \pi,\ 0 \le \Gamma \le w^*$, and $\theta' = 0,\ 0 \le \Gamma'; \le w^*$ $a = a^*$. On the other hand the current fluxes integrated over each electrode are equal because the short-circuited electrodes cannot accumulate macroscopic charges. In the conformal space this condition is expressed in Equation (10), since fluxes are conserved by conformal transformations.[2, 3e–g]

$$\int_0^{w^*}\left(\frac{\partial a}{\partial\theta}\right)_{\theta=\pi}\mathrm{d}\Gamma = \int_0^{w^*}\left(\frac{\partial a}{\partial\theta'}\right)_{\theta'=0}\mathrm{d}\Gamma' \tag{10}$$

Numerical evaluation of the gradients versus θ or θ' is performed through a three point parabolic approximation as previously reported. This amounts to express each of the above integrals as a linear function of a^*, so that the above equality affords a^* as a linear function of a values at selected mesh points of the finite difference grids used in each synaptic compartment. Based on the above procedures, the values of a (and of $b = 1 - a$) can be evaluated at each required mesh point for each value of the dimensionless time λ. From these concentration maps (e.g., as that shown in Figure 7b) the currents flowing through each electrode can be readily evaluated at any instant. Again, because of the conservation of fluxes through the conformal transformation, the current i_g at the input of the first synapse and that, i_c, at the output of the second synapse are given by the two following integrals performed in the conformal space[2, 3e–g] [Eqs. (11) and (12)], in which l is the common length of the electrodes in the real space.

$$i_g = nFD[Red]^{bulk}l\int_0^{w^*}\left(\frac{\partial a}{\partial\theta}\right)_{\theta=0}\mathrm{d}\Gamma \tag{11}$$

$$i_c = nFD[Red]^{bulk}l\int_0^{w^*}\left(\frac{\partial a}{\partial\theta'}\right)_{\theta=0}\mathrm{d}\Gamma' \tag{12}$$

Acknowledgments

This work has been supported in part by CNRS (URA CNRS 1679), by the Ecole Normale Supérieure and by MENRT.

[1] J. R. Monck, J. M. Fernandez, *J. Cell. Biol.* **1992**, *119*, 1395.
[2] C. Amatore, in *Physical Electrochemistry*, (Ed.: I. Rubinstein), M. Dekker, New York, **1995**, pp. 131–208.
[3] a) T. V. Shea, A. J. Bard, *Anal. Chem.* **1987**, *59*, 2101; b) J. E. Bartelt, M. R. Deakin, C. Amatore, R. M. Wightman, *Anal. Chem.* **1988**, *60*, 2167; c) K. Aoki, *J. Electroanal. Chem.* **1989**, *270*, 35; d) B. J. Seddon, H. H. Girault, M. J. Eddowes, *J. Electroanal. Chem.* **1989**, *266*, 227; e) B. Fosset, C. Amatore, J. E. Bartelt, A. C. Michael, R. M. Wightman, *Anal. Chem.* **1991**, *63*, 306; f) B. Fosset, C. Amatore, J. E. Bartelt, R. M. Wightman, *Anal. Chem.* **1991**, *63*, 1403; g) C. Amatore, B. Fosset, K. M. Maness, R. M. Wightman, *Anal. Chem.* **1993**, *65*, 2311; h) C. Belmont, H. H. Girault, *Electrochim. Acta* **1995**, *40*, 2505; i) T. A. Postlethwaite, J. E. Hutchinson, R. Murray, B. Fosset, C. Amatore, *Anal. Chem.* **1996**, *68*, 2951; j) C. Amatore**,** *C. R. Acad. Sci. Paris, Ser. II b* **1996**, *323*, 757.
[4] C. Amatore, A. R. Brown, L. Thouin, J. S. Warkocz**,** *C. R. Acad. Sci. Paris, Ser. IIc*, **1998**, *1*, 509.
[5] a) T. Horiuchi, O. Niwa, M. Morita, H. Tabei, *Anal. Chem.* **1992**, *64*, 3206; b) M. Morita, O. Niwa, T. Horiuchi**,** *Electrochim. Acta* **1997**, *42*, 3177.

0947-6539/99/0502-0464 $ 17.50+.50/0 *Chem. Eur. J.* **1999**, *5*, No. 2

[6] M. F. Bento, L. Thouin, C. Amatore, M. I. Montenegro, *J. Electroanal. Chem*. **1998**, *443*, 137.
[7] A. J. Bard, L. R. Faulkner, *Electrochemical Methods*, Wiley, New York, **1980.**
[8] a) R. C. Engstrom, C. M. Pharr, *Anal. Chem.* **1989**, *61*, 1099A; b) A. J. Bard, F. F. Fan, M. V. Mirkin, in *Electroanalytical Chemistry, Vol. 18* (Ed.: A. J. Bard), M. Dekker, New York, **1994**, pp. 243–373; c) A. J. Bard, F. R. Fan, M. Mirkin, in *Physical Electrochemistry*, (Ed.: I. Rubinstein), M. Dekker, New York, **1995**, pp. 209–242.
[9] See, for example: a) P. N. Bartlett, P. B. M. Archer, S. K. Ling-Chung, *Sensors and Actuators*, **1989**, *19*, 125; b) P. N. Bartlett, S. K. Ling-Chung, *Sensors and Actuators*, **1989**, *20*, 287; c) J. V. Hatfield, P. Neaves, P. J. Hicks, K. Persaud, P. Travers, *Sensors and Actuators B*, **1994**, *18–19*, 221; d) J. White, J. S. Kauer, T. A. Dickinson, D. R. Walt, *Anal. Chem*. **1996**, *68*, 2191; e) T. A. Dickinson, D. R. Walt, J. White, J. S. Kauer, *Anal. Chem*. **1997**, *69*, 3413; f) S. R. Johnson, J. M. Sutter, H. L. Engelhardt, P. C. Jurs, J. White, J. S. Kauer, T. A. Dickinson, D. R. Walt, *Anal. Chem*. **1997**, *69*, 4941.
[10] M. F. Bento, L. Thouin, C. Amatore, *J. Electroanal. Chem.* **1998**, *446*, 91.
[11] C. Amatore, A. R. Brown**,** *J. Am. Chem. Soc.* **1996,** *118*, 1482.

Received: July 8, 1998 [F1249]